

Diffraction Line-Shape Analysis of Poly(3-dodecylthiophene): A Study of Layer Disorder through the Liquid Crystalline Polymer Transition

T. J. Prosa,[†] J. Moulton,[‡] A. J. Heeger,[‡] and M. J. Winokur^{*,§}

National Institute of Standards and Technology, Gaithersburg, Maryland 20899, Department of Physics and IPOS, University of California, Santa Barbara, California 93105, and Department of Physics, University of Wisconsin, Madison, Wisconsin 53706

Received July 7, 1998

ABSTRACT: The nature of the structural ordering within semicrystalline poly(3-dodecylthiophene) films has been analyzed using a Warren–Averbach line-shape analysis which includes up to five orders of the (*h*00) lattice reflections. This analysis yields a semiquantitative measure of the volume averaged crystallite sizes, the lattice parameter variations, and the disorder fluctuations. The progression of these quantities has been followed through a liquid crystal polymer (LCP) phase transition which occurs in the vicinity of 60 °C. The pronounced peak width narrowing of the low-order (*h*00) reflections, observed on heating, is found to be essentially uncorrelated with a theorized annealing-induced increase in average crystallite size. The major contribution to this narrowing arises from systematic variations in the microscopic heterogeneities and fluctuations. Moreover, we observe an anomalously large increase in the higher-order (*h*00) (*h* = 3–5) peak widths at temperatures spanning that of the thermotropic LCP transition. This effect is found to be strongly correlated with a maximum in the disorder fluctuations, and this relationship suggests an underlying mechanism for the nature of the LCP transition.

Introduction

The increasing molecular-level complexity of polymeric materials, in the pursuit of specific nanoscale architectures and properties, has created a vastly expanding litany of possible structural forms possessing a wealth of subtle, contradictory, and often interrelated structural characteristics. In addition to the overall organizational features of the fundamental base structure, these systems often contain pronounced microscopic inhomogeneities indicative of paracrystallinity, structural defects, and/or systematic disorder. In many instances these secondary effects are an integral component of the molecular-level structure and, as such, necessarily play a fundamental role in defining a material's properties and limitations.

The poly(alkylthiophene) (or PAT) family of conducting polymers is a widely studied model system, and these hosts exhibit a diverse range of physical traits.^{1–3} Much of this behavior can be traced directly to the side-chain addition which fulfills a number of technologically important roles. Foremost is the creation of soluble and fusible materials which retain the electroactive nature of the conjugated polymer backbone. However, there is an array of secondary effects that are both electronic and structural in nature. The chemical incompatibility between the polar π -conjugated thiophene main chain and nonpolar alkyl side chains effects a constrained local phase separation whereby layered stacks of the main chains are separated by well-defined layers of the side chains. Thus, a series of evenly spaced reflections at low angle are clearly observed in diffraction studies, and these represent the first-, second-, and higher-order reflections of the lamellar *d*-spacing.⁴ This close stacking of the polythiophene backbones enhances the interchain transport and dramatically improves the measured

conductivities, especially in polymer compounds which are regioregular.⁵

The lamellar construction of these PATs also manifests a number of scattering attributes indicative of local disorder and strong structural heterogeneities, including paracrystallinity. These irregularities may be intrinsic (the presence of gauche conformations and side-chain packing disorder) or extrinsic (the extent of regioregularity of the side-chain anchoring). This disorder can be random in origin (i.e., uncorrelated), leading to the well-known Debye factor exponential drop in intensity with respect to higher order, or far more complex, as indicated by a systematic increase in the observed peak widths with higher-order index.⁶

A general procedure for analyzing the complex evolution of individual peak line shapes (including widths) was proposed by Hosemann assuming that polymers and other materials exist with a solid-state structure different than that of a perfect crystal.^{7–10} Instead of describing a solid as being composed of a three-dimensional (3D) crystalline lattice with statistical variations from the equilibrium positions, a better description is to employ an ordered array of unit cells that exist as distorted parallelograms. These parallelograms essentially retain the row and column structure but include significant amounts of distortion. The lattices of these "paracrystals" have distance statistics which can then be generated as shown by the specific examples cited in Hindeleh and Hosemann.⁷ As a result, imperfect materials often exhibit systematic effects in their Bragg scattering profiles which can be quantified through a detailed line-shape analysis of the individual Bragg reflections.¹¹

In a traditional line-shape analysis, the observed profiles result from a convolution of various broadening mechanisms including a distribution of finite crystal sizes (coherently diffracting domains or CDDs), variation in lattice parameters from CDD to CDD, and displacement disorder within a CDD. The effects of

[†] National Institute of Standards and Technology.

[‡] University of California.

[§] University of Wisconsin.

crystal size are independent of the order for a given series of reflections, whereas lattice parameter fluctuation and displacement disorder both impart a functional dependence with respect to the order for a given set of reflections. For materials whose x-ray diffraction profiles exhibit multiple orders of a given reflection [such as (100), (200), ...], the effects of crystal size and disorder can, in principle, unambiguously be separated. In practice, the problematical nature of polymer scattering often makes this approach a difficult proposition. The basic origins of this technique are credited to Warren and Averbach (WA) who applied this analysis to metals having undergone mechanical deformations.^{6,12-14} This analysis continues to be applied to scattering from metals and superconductors,¹⁵⁻²³ ceramics,^{24,25} and other materials.²⁶ These systems tend to have large CDDs and relatively small, unambiguous scattering backgrounds as compared to most polymers. In these materials, corrections for instrumental effects are the primary difficulty and erroneous background subtraction is a secondary concern limiting the final accuracy of extracted quantities.

Application of the WA approach to polymer systems has had some limited successes.^{11,27-29} The difficulties in determining the correct noncrystalline background, which can account for an appreciable component of the scattering, and a pronounced lack of multiple diffraction peak orders are the two major factors limiting a direct application of the WA method to analyzing polymer microstructure. Layer-forming polymers, especially those with a well-defined layer d -spacing are potentially useful candidate materials in this respect because the Bragg reflections arising from the large d -spacing can be reasonably well-segregated from other reflections and each other. Poly(3-dodecylthiophene) (P3DDT), which has a nominal 26.2 Å layer room temperature d -spacing, five (or more) distinguishable ($h00$) orders, and pronounced signatures of local disorder, is an attractive system for a rigorous separation of size and disorder effects via the WA analysis.

The semicrystalline nature of P3DDT (and many other PATs) has been studied extensively by x-ray diffraction;^{2,30} as well as by many other techniques^{1,31-34} [including UV absorption, differential scanning calorimetry (DSC), and infrared spectroscopy], and the thermotropic evolution of the semicrystalline poly(3-alkylthiophene) (P3AT) films is qualitatively understood. DSC studies have revealed that P3DDT samples similar to those used in this study have two broad endothermic peaks at intermediate temperatures of ~30 and ~60 °C and then melt completely above 130 °C. The 30 °C peak has been attributed to a melting of the side-chain crystallinity, whereas the 60 °C transition is liquid crystalline in nature, whereby the "out-of-phase" staggering (parallel to the chain axis) by nearest-neighbor P3AT chains is lost, creating a nematic, free-floating, intrastack ordering. X-ray diffraction studies probing this transformation observe a progressive loss in scattering intensity in the (002) meridional peak³⁵ and a systematic merging of the various ($h20$) reflections³⁶ into a single broad scattering feature. The melting transition of the side chains and the loss of chain-to-chain stacking order appear to be correlated.

The majority of the above-cited x-ray studies are consistent with P3DDT adopting, at temperatures below 30 °C, a well-defined lamellar structure in which both the skeletal backbone and the alkyl side groups have

almost fully extended trans conformations. Detailed model calculations³⁶ support a structure in which the side chains are strongly tilted with respect to the layer repeat direction so that the side-chain nesting approximates a 4.5 Å hexagonal close-packing in close correspondence to the average packing of pure alkanes³⁷ or polyethylene.³⁸ Evidence for a secondary crystalline ordering of the side chains is seen in the methylenes farthest from the backbone. P3ATs with side-chains of octyl and shorter do not show this side-chain crystallization. This is evident from DSC and x-ray diffraction studies of P3ATs with various lengths of side chains. Earlier studies of other side-chain-substituted polymers support a model in which side-chain crystallinity begins at or near the 10th methylene group within the side chain.³⁹

In many instances, the (100) and higher-order ($h00$) reflections narrow somewhat at temperatures just above those spanning the thermotropic liquid crystal phase (LCP) transitions.^{35,36,40} For P3DDT, a claimed ~15% increase in crystal size (over the temperature range of 10–120 °C) is obtained by applying the methodology of Scherrer⁴¹ which simply examines the individual peak full width at half-maximum (fwhm). However, it is important to emphasize that this often-used Scherrer analysis is known to constitute only a *rough* measure of this quantity and, as a result, many claims of the measured CDD dimensions are actually overestimates (up to a factor of two).

In this paper, after a brief review of WA line-profile analysis theory and necessary methodology, we apply this method to analyze the ($h00$) reflections observed in uniaxially stretch-oriented P3DDT as a function of temperature. This WA analysis clearly demonstrates that the vast majority of observed narrowing in any of the ($h00$) diffraction profiles is not associated with increases in the mean crystallite size. In fact, much of the inferred narrowing is actually correlated with a pronounced ($h00$)-order-dependent peak *broadening* anomaly which spans the temperatures between the broad DSC endotherms observed at ~30 and ~60 °C. This structural evolution is overwhelmingly dominated by a singular and systematic reduction in the lattice parameter fluctuation and a pronounced increase in the disorder fluctuations at temperatures near the LCP transition temperatures. Changes in side-chain disorder are inferred by considering the disordering mechanisms present in P3DDT in a direction perpendicular to the polythiophene polymer axis and that of the polymer layers (i.e., along the layer repeat direction). A possible explanation for this increase in the disorder fluctuations at intermediate temperatures appears to be rooted in the existence of a highly heterogeneous melting of the alkyl sidechains and, as such, may be a general attribute of LCP transitions in other structurally related polymer materials.⁴²

Experimental Section

The P3DDT samples utilized in this study were obtained by a direct oxidative coupling of 3-dodecylthiophene with FeCl₃.⁴³ After synthesis, the FeCl₃ was extracted, and the films were dissolved in chloroform. These solutions were then filtered and immediately poured directly onto glass slides. After solvent evaporation, the films were lifted by methanol and clamped into a simple stretching device. Uniaxial stretching ratios approaching 4:1 were achieved at drawing temperatures

of ca. 100 °C, producing film thicknesses of approximately 40 μm .^{44,45} These samples were then stored in a clamped state at room temperature for a number of months. Both casting and uniaxial stretching introduced anisotropy in the spatial distribution of the crystallite fractions so that a full 3-dimensional texturing is obtained.³⁶ Because regioregularity of a side-chain anchoring site can be an important issue, we note that these P3DDT samples exhibit an approximate 75% head–tail coupling of the 3-alkylthiophene monomers to the main chain.⁴⁶

The primary x-ray instrumentation utilized in this study included a rotating anode generator with a copper target ($\lambda_{\text{K}\alpha} = 1.542 \text{ \AA}$), an elastically bent LiF monochromator, an INEL CPS120 “wire” detector designed around a blade anode (which allows for a simultaneous 120° 2θ of data acquisition with 0.015° readout resolution), and full helium beam paths to minimize “air” scatter.⁴⁷ The polymer sample was mounted in transmission geometry and placed in a heater cell assembly stabilized to better than $\pm 2 \text{ }^\circ\text{C}$. Initially, the sample was cooled to 10 °C using a water-cooled peltier stage (Melcor Frigichip CP1.0–31–05C). Temperatures were increased in a stepwise fashion (from 10 to 30, 50, 60, 70, 80, 100, and finally 120 °C). At each temperature, the sample was allowed to equilibrate a minimum of ~ 15 minutes before the continuation of data acquisition. Acquisition times varied from 4–8 hours, with typically 2×10^7 counts recorded across the entire detector array.

Subsequent long-term detector background studies using a Fe⁵⁷ source revealed systematic and reproducible pixel-to-pixel relative intensity variations of up to 0.5%. This nonlinearity of response has been found to drift very slowly over long time frames and thus limits the ability for a full retroactive correction of this effect. At the time of data acquisition, a reliable method for correction of this systematic error had not been fully implemented, thereby limiting this component of relative standard uncertainty to 0.5% (or less).

Data sets were corrected for instrumental broadening by the method of iterative unfolding.⁴⁸ A zeolite powder sample, Y-52, was used as an instrumental standard. Resulting scattering profiles exhibited 13 strong, non-overlapping peaks in the range 6.0°–32.0° 2θ . The absence of a zeolite peak near $\sim 3.3^\circ 2\theta$ required an extrapolation of instrument peak parameters to this scattering region.

Each zeolite reflection was fit with two pseudo-Voigt shaped peaks, $\eta G + (1 - \eta)L$ (where G and L are Gaussian and Lorentzian peaks with the same full width at half-maximum), to reproduce the partially superimposed K_{α_1, α_2} character for each instrumental peak. The measured peak widths were then fit^{49,50} to $\text{fwhm}^2 = U \tan^2 \theta + V \tan \theta + W$, with average values of $\eta_{\alpha_1} = 0.60$, $\eta_{\alpha_2} = 0.74$, and α_1/α_2 intensity ratio of 3.33, remaining relatively constant over the region of interest. This procedure allows one to approximate the “instrumental” broadening effects present at every 2θ position in the data sets.

Line-Shape Broadening

A. General Overview. In the absence of instrumental contributions, all observed diffraction profiles must be representative of a convolution of at least three nominally independent broadening mechanisms: the CDD size (i.e., crystal size), “long-range” disorder including lattice parameter fluctuations, and paracryst-

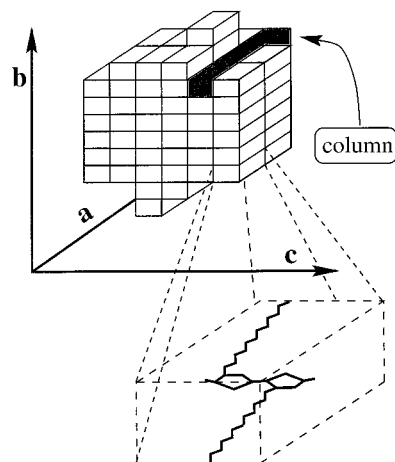


Figure 1. Representation of the poly(3-dodecylthiophene) crystal packing by considering it to be composed of *columns* of unit cells parallel to the *a*-axis.

talline displacement disorder (of the second kind). Each of these attributes imparts a different order-dependent functionality and, in the presence of at least two or more resolved orders of reflection, can be uniquely specified. The exact microscopic origin of the latter two displacement fluctuations are varied and have been the subject of much debate but, for the purposes of this work, are not a priori specified in any overt fashion. The actual process of deconvoluting these peak broadening mechanisms is further complicated by moments in the broadening mechanism distributions which give rise to pseudo-Voigt line-shapes. Although cumbersome, the general methods of WA,^{6,12–14} and more specifically the methodology utilized by Crist and Howard in a polyethylene study,²⁹ allow these effects to be individually resolved.

Displacement disorder of the first kind can be characterized as displacement defects or physical defects that disturb the “short-range” order within a crystallite. This type of disorder manifests itself as thermal vibrations, frozen displacements, or other phenomena that do not alter the actual shapes of any Bragg diffraction peak but do influence the intensity as a function of scattering angle.⁴¹

Prior to implementing a WA line-shape analysis, all data must be first corrected for effects not reflected in the internal structure of the material. Examples of these include instrumental broadening, Lorentz-polarization factors, and variations in atomic scattering and absorption. After the appropriate correction procedure, the n th-order Fourier cosine transform coefficient of a specific h -order diffraction peak has the form^{6,29,51,52}

$$A_h(n) = A^S(n)A_h^e(n)A_h^D(n) \quad (1)$$

$$L(n) = n/N\Delta q \quad (2)$$

where $A^S(n)$, $A_h^e(n)$, $A_h^D(n)$ are the normalized [$A_h(0) \equiv 1$] Fourier cosine coefficients for, respectively, the crystallite size, lattice parameter fluctuation, and displacement disorder. The Fourier coefficients with $n = -N/2, -N/2 + 1, \dots, N/2$ contain information on a length scale $L(n)$ which is dependent on the angular distance between scattering points, Δq , and number of scattering data points, N , considered for a given Bragg peak.

The line broadening problem has been traditionally considered using an arbitrary distribution of crystal-

lites,¹⁴ whereby each crystallite can be represented in terms of a 2-dimensional array of columns of unit cells along some \vec{a} direction (see Figure 1). The statistical description of the various broadening mechanisms is straightforward and is thoroughly discussed by Crist and Howard.²⁹ The lattice parameter $d = |\vec{a}|$, which defines the average lattice spacing within a particular crystallite, and $\langle d \rangle$ which defines the average lattice parameter value averaged over all crystallites, allows one to define the lattice parameter fluctuation reduced variance as

$$\langle e^2 \rangle = (\langle d^2 \rangle - \langle d \rangle^2) / \langle d \rangle^2 \quad (3)$$

Likewise, Z_n describes the displacement between two unit cells within a column that are n unit cells apart, with an ideal separation of nd and an actual separation of $n\vec{d}$. Takahashi⁵¹ has argued that strain distributions with identical particles and independent displacements of unit cells can be regarded as the sum of a finite number of random variables with the following relation expected:

$$\langle Z_n^2 \rangle = n \langle Z_1^2 \rangle = n (\langle \vec{d}^2 \rangle - \langle d \rangle^2) / \langle d \rangle^2 = n g^2 \quad (4)$$

The linear dependence of $\langle Z_n^2 \rangle$ on n can be shown to result from various types of displacement disorder of the second kind.^{51,53-55} The fact that the reduced positional uncertainty increases with separation is the signature of this type of disorder.

The normalized Fourier cosine coefficients should then be of the following form:¹⁴

$$A^S(n) = N(n)/N_3 \quad (5)$$

$$A_h^e(n) = \langle \cos(2\pi h n e) \rangle \quad (6)$$

$$A_h^D(n) = \langle \cos(2\pi h n Z_n) \rangle \quad (7)$$

where $N(n)$ is the average number of crystal cells $L(n)$ apart per column of cells (each cell extends parallel to the layer normal direction \vec{a}). N_3 is the volume-averaged column length, or the effective average crystallite size. Equations 6 and 7 can be expanded with no loss of generality

$$A_h^e(n) = 1 - 2\pi^2 h^2 n^2 e^2 + \mathcal{O}(\Delta) - \dots \quad (8)$$

$$\approx e^{-2\pi^2 h^2 n^2 e^2} \quad (9)$$

$$A_h^D(n) = 1 - 2\pi^2 h^2 n^2 \langle Z_n^2 \rangle + \mathcal{O}(\Delta) - \dots \quad (10)$$

$$\approx e^{-2\pi^2 h^2 n^2 \langle Z_n^2 \rangle} \quad (11)$$

with approximated eqs 9 and 11 being valid for small fluctuations or exact for fluctuations obeying Gaussian statistics.

Following the graphical method of WA^{6,12} and Crist and Howard²⁹ (see Figure 2), one can separate size and distortion effects by taking the natural logarithm of eqn 1:

$$\ln A_h(n) = \ln N(n)/N_3 - 2\pi^2 h^2 n f(n) \quad (12)$$

$$f(n) = g^2 + n \langle e^2 \rangle \quad (13)$$

Applying linear regression to a "Guinier" plot of $\ln A_h(n)$ versus h^2 , while holding n constant, determines the

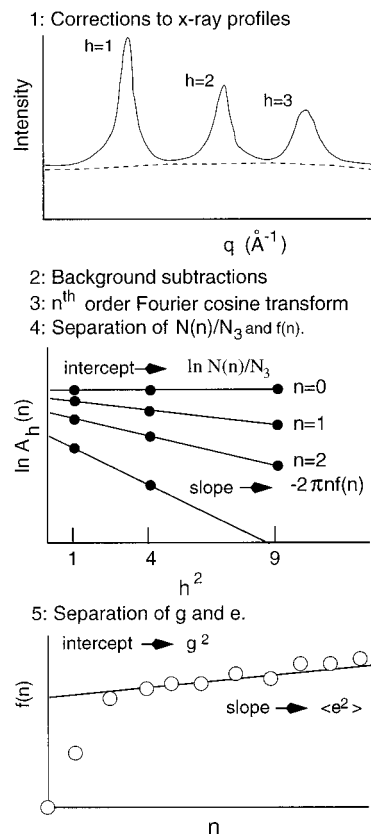


Figure 2. Schematic of peak profile analysis methodology.

terms $\ln N(n)/N_3$ and $-2\pi^2 f(n)$ from the y -intercepts and slopes, respectively. Thereafter, one can further separate the effects of lattice parameter and displacement disorder by a linear regression analysis of $f(n)$ versus n or, equivalently, $f(L)$ versus L , where L is given by eq 2.

Errors in background determination and Fourier transformation, especially those resulting from the truncation of experimental diffraction peak tails, can lead to misrepresentation of the lowest-order Fourier coefficients. Regrettably, these are the same coefficients that are the most accurately approximated by eqs 9 and 11. These errors are evident when a plot of $\ln A^S(n)$ versus n possesses any negative curvature. This "hook effect" is not physically allowable because the volume-weighted distribution of column lengths, $p_v(n)$, is related to the second derivative of the crystal size coefficients, $A^S(n)$, by the relation⁵⁶⁻⁵⁹

$$n p_v(n) = \frac{d^2 A^S(n)}{dn^2} \quad (14)$$

In general practice, when the hook effect is present, the lowest-order coefficients are ignored (in our case, for $n \leq 3$), and a linear fit of $f(n)$ versus n returns the values for $\langle e^2 \rangle$ and g^2 .

When disorder fluctuations are not small or when distributions do not exhibit Gaussian statistics, eqs 9 and 11 may not remain reliable approximations. This problem can be overcome with the availability of more than two orders of reflection, allowing for the implementation of the more general expansion

$$A_h(n) = \frac{N(n)}{N_3} \left[1 - \frac{4\pi^2 h^2 n}{2!} (g^2 + n\langle e^2 \rangle) + \frac{16\pi^4 h^4 n^2}{4!} (g^4 + 2n\langle e^2 \rangle g^2 + n^2\langle e^4 \rangle) - \dots \right] \quad (15)$$

Alternatively, fitting $A_h(n)$ to $a_n - b_n h^2 + c_n h^4 - \dots$ also allows for the separation of size and distortion effects from peak profiles,⁶⁰ where $N(n)/N_3 = a_n$ and $f(n) = b_n / 2\pi h^2 n a_n$.

B. Procedure for Polymer Peak Analysis. After iteratively unfolding the instrument profile from the diffraction spectra, the raw data sets (shown in Figure 3) were corrected for Lorentz polarization, absorption, variations in atomic scattering, and Debye–Waller effects.⁴¹ Conversion from 2θ to wave vector, $q = (4\pi/2)(\sin \theta)/\lambda$, was immediately followed by subtraction of an appropriate background. Each data set was fit with a linear superposition of pseudo-Voigt peaks that approximated scattering by both “amorphous” and crystalline scattering sources (the background profile for the 10 °C P3DDT data is illustrated in Figure 4). To obtain a single peak line-shape, a composite of the amorphous background profile and all other fitted crystalline peaks was subtracted from the experimental data. Thus, the overlapping effect of neighboring diffraction peaks was addressed by effectively treating them as a background feature in extracting the particular peak profile of interest.

The choice of an appropriate background is especially important. Some studies have used profiles from samples quenched from the melt as a background for subsequent line-shape analysis. The overall efficacy of this method in polymers is suspect because of the sensitivity of polymer structure to forming conditions. For these P3DDT samples, this approach could not be implemented.

To place some constraints on the actual backgrounds used, two considerations were emphasized. First, a prior structure factor modeling study was used to formulate acceptable crystalline and amorphous scattering fractions,³⁶ and second, the known existence of a second structural polymorph (a type-II phase) provided for the inclusion of additional narrower features in the background profile.⁶¹ These features have been observed in a variety of P3AT samples.^{61–65} The presence of this minority phase impurity produced three modest intensity localized features, centered at 2θ values of 4.75° , 9.5° , and 14.2° (identified by arrows in Figures 3 and 4).

One final experimental artifact, arising from a combination of the broad character of the $(h00)$ diffraction peaks, the large interlayer d -spacing, and the associated small angle of the (100) reflection, created an unavoidable “shadowing” of the beam stop over the low-angle portion of the (100) peak. Corrections for the (100) peak intensity at 2θ angles less than 3° were obtained by simply mirroring the unaffected line-shape from the high-angle side.

A fast Fourier transform (FFT) algorithm⁶⁶ was implemented to perform the necessary transforms. To minimize the introduction of truncation effects for the Fourier coefficients of interest, tails were added to the resulting peak profiles.⁶⁰ Each peak was fit to a pseudo-Voigt line-shape, and the tails from this function were added where data values approached 0 to within the error of the data (an example is illustrated in Figure 5). All imaginary parts of the resulting transforms (sine

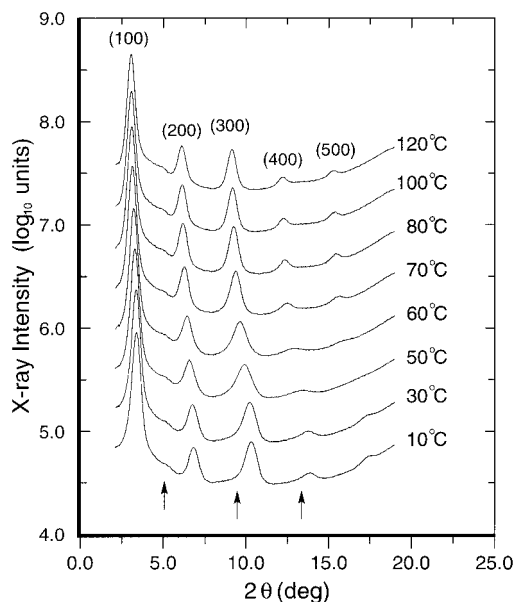


Figure 3. Plot of equatorial P3DDT scattering data showing the relative intensity variation for the first five $(h00)$ orders of the interlayer repeat. Arrows indicate positions of parasitic secondary peaks from crystalline structural polymorph (type-II).

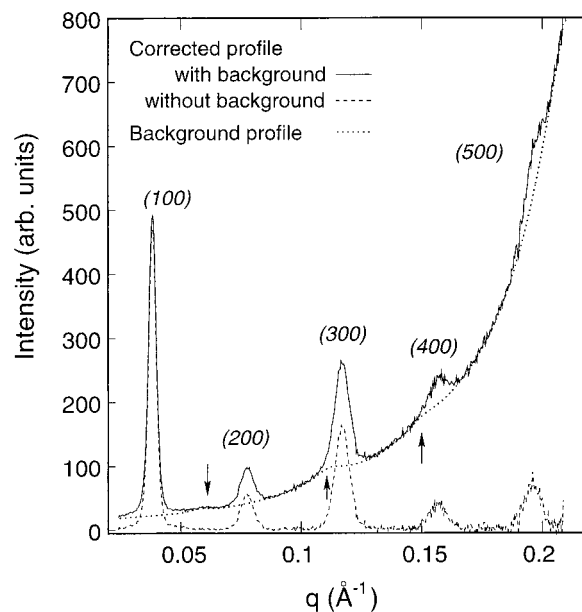


Figure 4. Corrected 10 °C data set before and after background removal. Relative uncertainties are less than 0.5%. Note: In this instance $q \equiv 2(\sin \theta)/\lambda$ which is conventional in peak shape analysis.

coefficients) were within expected limits due to counting statistic limitations and therefore negligible, but to insure that the above manipulations of the various diffraction profiles had not resulted in an unphysical peak shape (assuming mirror symmetry of the peaks), the real part of the transforms was inverse-transformed and subtracted from the original data, revealing what can be considered as the “true” background used in this analysis. The resulting transforms were then fit by both eqs 12 and 15, yielding numerical values for the aforementioned broadening parameters.

Results and Discussion

A stepwise thermal progression of eight equatorial P3DDT scattering profiles, before application of any

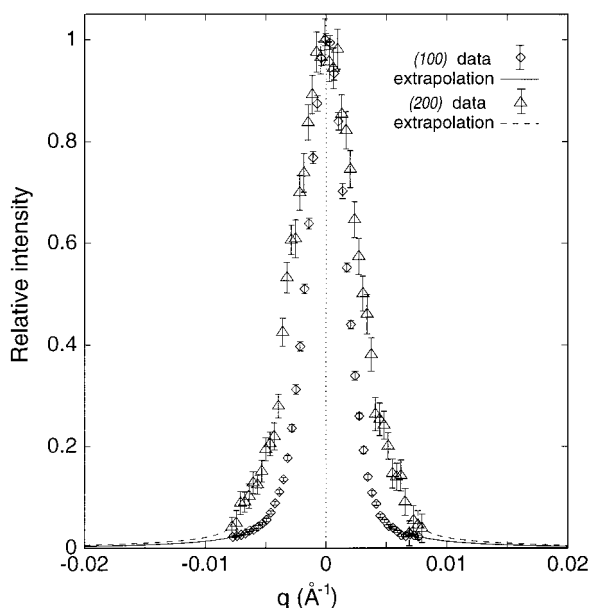


Figure 5. Two 10 °C ($h00$) experimental curves in combination with added "wings" (or "tails") for reduction of FFT artifacts. Error bars represent 95% confidence levels based on combinations of the counting statistics.

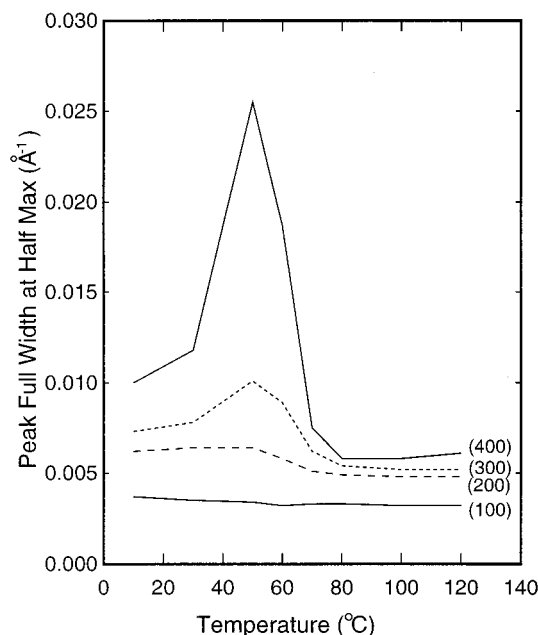


Figure 6. Variations in measure peak full width at half-maximum for the indicated ($h00$) reflections.

corrections or background subtraction, is shown in Figure 3 using a \log_{10} scale. In these curves, the first five ($h00$) Bragg reflections are clearly discernible, and the qualitative changes in the peak behavior are evident. With respect to the two limiting temperatures, 10 and 120 °C, the systematic narrowing on heating is clearly demonstrated.

To emphasize the systematic complexity in the evolution in response to thermal heating, every peak full width at half-maximum for the first four ($h00$) reflections is plotted in Figure 6. The (100) reflection tends to narrow smoothly with increasing temperature so that a simple Scherrer analysis suggests a modest increase in the average crystallite size from 270 to 310 Å. With the exception of the (100) reflections there is a dramatic temperature-dependent *broadening* of the high-order

Table 1. Table of Relative Gaussian/Lorentzian Line-Shape, η

temp (°C)	$h = 1, \eta$	$h = 2, \eta$	$h = 3, \eta$	$h = 4, \eta$
10	0.60	0.77	0.83	0.63
30	0.61	0.74	0.81	1.00
50	0.61	0.16	0.33	0.38
60	0.58	0.10	0.30	0.06
70	0.58	0.63	0.25	0.84
80	0.64	0.78	0.45	0.02
100	0.59	0.64	0.45	0.36
120	0.62	0.57	0.45	0.00

reflections at temperatures from 30 to 60 °C; the higher the h index, the more pronounced the broadening becomes. In the case of the (500) reflection, labeled in Figure 3, this peak is only marginally discernible over the background in the 50 °C scan.

With respect to the WA analysis, the elimination of effects arising from the unwanted type-II minority phase peaks was, in certain instances, especially troublesome. Although the first of these peaks was located almost halfway between the (100) and (200) reflections, making its removal straightforward, the second- and third-order type-II phase peaks are positioned immediately adjacent to or underneath the (300) and (400) profiles. Because of differences in the thermal expansion of these two phases, the second-order background peak (indicated by the arrow at $\sim 9^\circ 2\theta$) starts out on the low-angle shoulder of the (300) peak at 10 °C and effectively shifts toward the higher 2θ angle, until it has nearly the same scattering angle as the (300) peak, at 60 °C. This systematic behavior strongly inhibited an unambiguous determination of the peak profiles in the (300) reflection over this temperature range. Still, the line-shape progression with increasing order specified by eqs 12 and 13 allows one to choose only backgrounds which give rise to physically meaningful parameters. Without this limiting constraint, the resulting crystal size and disorder parameters became intolerably large, and the lattice parameter fluctuations appeared unphysical (i.e., negative). For temperatures above 60 °C, the type-II phase transforms into the majority phase, thereby significantly simplifying the background-fitting procedure. Moreover, at these higher temperatures, the 5th-order peak was sufficiently well-resolved for inclusion in the WA analysis.

Despite these difficulties, the presence of multiple, resolvable ($h00$) reflections both lessens the negative impact that an inaccurate peak profile imparts on final disorder parameter values and, simultaneously, provides insight as to the correct peak profile by imposing a self-consistent progression of peak profiles with respect to increasing h -order. Table 1 contains the extracted pseudo-Voigt functionality of various peak line-shapes, η , as a function of temperature and increasing h -order. Although the relative fluctuations in η are significant, especially those of $h = 3$ and 4, there is ample evidence for systematic behavior. In the case of the (100) reflection, η is essentially temperature-independent with an average value of approximately 0.60 (a more Gaussian-like line-shape). With respect to fixed temperature and increasing h -order, there is a gradual evolution towards a predominantly Lorentzian character at temperatures above 70 °C and a weak tendency towards increased Gaussian character for temperatures below 50 °C. In the two intermediate temperature scans, there is a rapid drop to a Lorentzian dominated profile on stepping from the (100) to the (200) reflection.

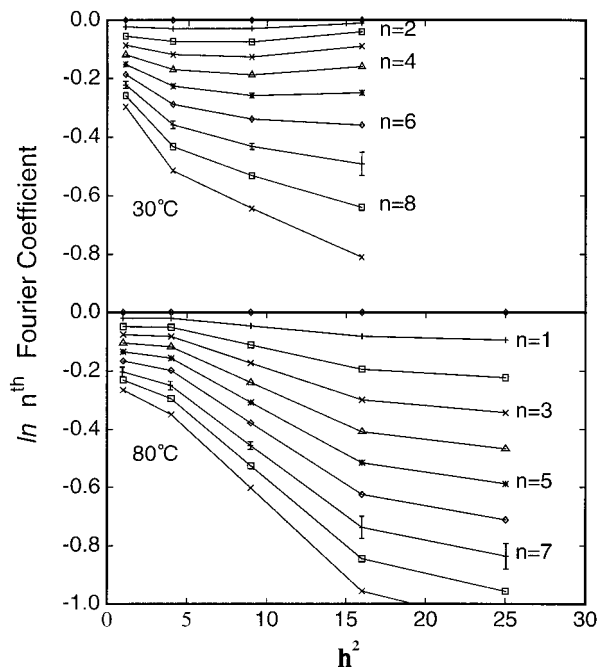


Figure 7. P3DDT Fourier cosine coefficients for the first four or five orders of the ($h00$) reflection vs h^2 for temperatures of 30 (top) and 80 °C (bottom).

The presence of five orders of reflection also highlights the potential problems implicit in studies that include only a small number of reflection orders. When applying the Warren–Averbach/Crist–Howard method to P3DDT diffraction spectra using only the first two orders of reflection, the separation of size and fluctuation effects is trivial (two points make an unambiguous line). When the (300) peaks are considered, a plot of $\ln A_h(n)$ versus h^2 quite frequently appears nonlinear, nondecreasing, or both (see Figure 7); although this is consistent with studies of other materials.^{12,67,68} If higher-order peaks are utilized, the break from nonlinearity is even more pronounced. This suggests that the approximations used in eq 12 may be breaking down even before the 3rd-order reflection and that higher moments of Z_n are becoming important or, possibly, that errors in background subtraction have occurred. Few authors have commented on deviations from the expected linear relationship between peak shape and peak order correlations, and we are aware of only two prior polymer studies which include three⁶⁷ or more⁶⁸ orders within a family of reflections.

Using all available data from the Figure 7, four orders for temperatures below 60 °C and all five orders otherwise, and separating size and distortion according to the approximations implicit in eq 12 results in size coefficients with little or no hook effect. Estimates of Fourier coefficient uncertainties were consistently determined and used so that, in effect, the higher-order coefficients ($h > 2$) often had only a limited impact on the final results. The resulting plot of $f(L)$ versus L , as shown in Figure 8, produced a linear relationship (except, as expected, for the lowest n -order coefficients), making separation of g and e straightforward and unambiguous. Fitting only the first three orders with eq 12 had little effect on N_3 but had some influence on the values of e and g .

When more than two orders of reflection are considered, higher-order terms are also available for separating the size and fluctuation coefficients through eq 15.

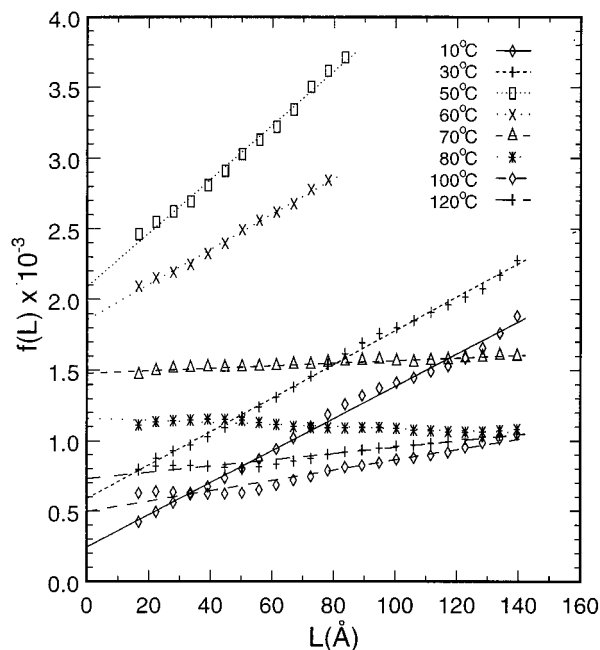


Figure 8. Plot of $f(L)$ vs L as obtained from eq 12. The slope and the y -intercept give $\langle e^2 \rangle$ and g^2 , respectively.

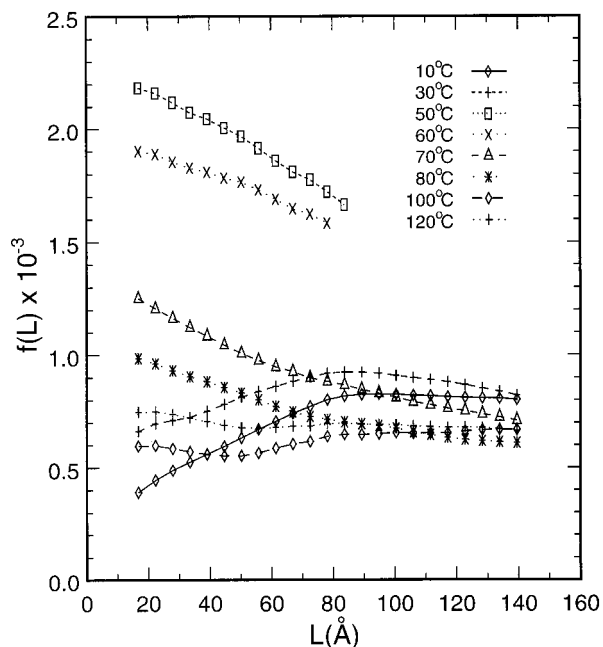


Figure 9. Plot of $f(L)$ vs L as obtained from eq 15. The slope and the y -intercept give $\langle e^2 \rangle$ and g^2 , respectively.

Moreover, if the coefficients are small, then both should yield similar results. Using this alternate method by fitting the data to eq 15 produced a better multiorder fit, but this is expected at the onset because this step introduces an additional fitting parameter. We note that the two representative Fourier coefficient versus the h^2 plots of Figure 7, at 30 and 80 °C, present somewhat different functional forms. In general, this method yielded size coefficients similar to those of the first scheme but typically gave comparatively smaller values of e and g . For some temperatures, the values of e and g simply could not be determined because plots of $f(L)$ versus L , as shown in Figure 9, possess a significant negative slope. Without improved scattering data, increased accuracy, or both in the background determi-

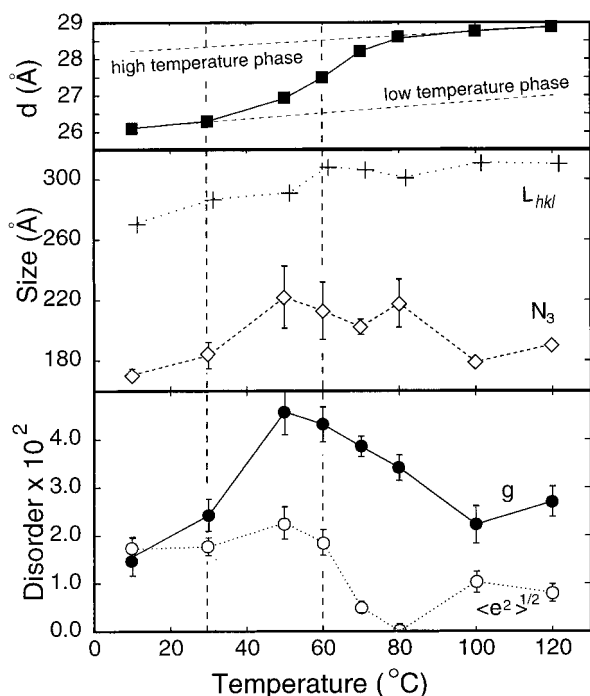


Figure 10. Plots of various parameters as a function of temperature for (at top) interlamellar d -spacing (■); (at middle) crystal size according to Scherrer formula (+) and WA analysis (\diamond); and (at bottom) displacement disorder, g (●), and lattice parameter fluctuation, e (○). Error bars represent 95% confidence levels based on a Monte Carlo bootstrap procedure.

Table 2. Peak Profile Analysis Results

temp (°C)	d (Å)	N_3 (Å)	g	e
10	26.1	171	0.016	0.017
30	26.3	183	0.024	0.018
50	26.9	222	0.046	0.023
60	27.5	213	0.043	0.019
70	28.2	202	0.038	0.005
80	28.6	218	0.034	0.000
100	28.8	179	0.022	0.010
120	28.9	190	0.027	0.008

nation, this approach will not yield additional improvements in the derived parameters.

The temperature dependence of the lattice parameter fluctuations, $\langle e^2 \rangle^{1/2}$, the disorder fluctuations, g , the CDD (N_3), and lattice repeat spacings (d) are all simultaneously displayed in Figure 10 and Table 2. When all broadening effects are taken into account, the Scherrer formula derived [$L_{hkl} = 0.89\lambda/\Delta 2\theta \cos \theta$ from the (100) data] average crystal size of 270 Å, at room temperature, drops to a nominal value of 170 Å. This disparity between the two methods can be attributed to a disproportionately high proportion of small crystallites within the polymer film. The scattering from these smaller crystals tends to produce contribution in the tails of the diffraction peaks without broadening the peak width proportionally. In fact, after the actual thermal expansion of the polymer unit cell is considered, this average 270 Å crystallite size remains a relatively constant function of temperature at approximately 10.5 lattice repeats. Thus, the narrowing in the observed (100) P3DDT peak width on increasing temperature, which has been attributed to an increase in crystal domain size,³⁵ appears to be a misleading conclusion.

The WA peak profile analysis presented here suggests a very modest increase in N_3 on moving from 10 to 50 °C. This may indicate an increase in crystal size from

6.5 to 7.5 unit cells although the subsequent drop in N_3 at even higher temperatures (where the background determinations are best) tend to implicate artifacts in the analysis procedure. In a more general setting, it is likely that analogous observations in other polymer hosts has led to similar misinterpretation of "annealing" in other polymer systems. Thus, many claims of increased or decreased crystal domain size may actually arise from irreversible (or possibly even reversible) reductions in the intrinsic disorder.

In contrast, the overall progression in the lattice parameter and disorder fluctuation is quite remarkable. As the temperature increases past the lower temperature DSC endotherm (~ 30 °C), the disorder fluctuations increase rapidly reaching a maximum near the higher temperature endotherm (~ 60 °C) which is nearly 3 times that measured at 10 °C. Further temperature increases are correlated with only gradual decreases in g . On the other hand, the lattice parameter fluctuation value remains relatively constant until after 60 °C and then drops to essentially zero before increasing once again. We stress that the results obtained at the highest temperatures are particularly free from uncertainties in the background determination and are therefore expected to be most accurate.

Without referring explicitly to this WA analysis, the simplest phase-transition sequence which could adequately explain the anomalously large increase in peak width as a function of increasing h -order, at 50 and 60 °C, would be that individual crystallite domains sequentially undergo a transformation to the LCP mesophase. In this case, these P3DDT samples would yield heterogeneous system having a two-phase coexistence of both the high- and low-temperature phases over an extended temperature range. Thus, the scattering profiles should be represented by a superposition of monotonically increasing/decreasing contributions of the two relative phase fractions possessing two different thermal expansion rates (see the top panel of Figure 10). The experimental data clearly contradicts this theorized scenario because only a *single* well-defined set of multiple higher-order peaks is ever recorded. The relatively narrow width of the peaks at temperatures straddling the two phase transitions in combination with the rather large difference in measured d -spacings would invariably create higher order ($h00$) reflections with a pronounced double-hump character.

Hence, we suggest the following sequence of events. At temperatures above the side-chain melting temperature (i.e., ~ 30 °C) there is a progressive loss of layer-to-layer coupling, and in addition, there is the onset of the chain-to-chain intrastack disordering transition. With respect to the first process, there appears to be a localized, uncorrelated melting of the side chains within each and every P3DDT crystallite. These local inhomogeneities apparently play a highly disruptive role in the development of periodic long-range order and, as such, would be expected to generate an extremely strong signature indicative of fluctuation disorder, especially with the approach of the second structural transition. At temperatures exceeding 60 °C, the nematic free-floating nature of the LCP system would tend to completely minimize any nonlocal impact of any residual inhomogeneities, thus allowing for a rapid decrease in the measured lattice parameter fluctuation and displacement disorder coefficients, at least until the onset of the higher temperature melting transition. This

process is probably rather general to lamellar LCP systems (including Langmuir–Blodgett multilayers), but we are presently unaware of any other studies attempting to obtain a rigorous result.

Conclusions

Although peak profile analysis has not been extensively applied to analyzing disorder in polymer structure, the lack of other available methods capable of quantitatively evaluating microstructure at this length scale suggests that more frequent use of a WA-like analysis is warranted. Although the topic of paracrystallinity and disorder in these less perfectly ordered systems (i.e., polymers) has been extensively discussed in theory, many discrepancies between theory and practice are still evident. In particular, the inability to obtain, independent amorphous background profiles for subsequent peak profile determination does lend some doubt as to the reliability of this technique for studying semicrystalline polymers. Yet, the present study has demonstrated that many of these difficulties can be overcome when suitable conditions exist.

The Fourier analysis of multiple peak profiles provides a straightforward procedure for separating the major peak broadening mechanisms, namely the effects of crystal size and disorder. This analysis has shown that crystal size, lattice parameter fluctuation, and displacement disorder of the second kind are all important factors in determining the peak shape of P3DDT. Although this parameterization is a convenient approach, there are important caveats. Polymers can be highly disordered heterogeneous systems. Hence this simplistic description of three generic line broadening processes ignores much of the microscopic realities of polymer structure. For example, distortions within crystallites would be expected to increase when traversing from the interior to the exterior of a crystallite although the actual point at which the crystallite ends (and amorphous region begins) may not be clearly differentiated. Nonetheless, more studies on similar polymer systems should be done to verify whether or not other materials exhibit analogous variations in these parameters. Obvious candidates are side-chain substituted materials, similar to P3DDT, that have increased side-chain crystallinity. These large *d*-spacings provide for multiple peak profiles that are relatively easy to distinguish from the amorphous background.

This peak profile analysis has revealed much about the variation of crystal size, lattice parameter fluctuation, and displacement disorder within P3DDT as a function of temperature. The significant overestimation of crystal size by applying Scherrer methodology has been demonstrated, with changes in crystal size being best described as a thermal expansion of the average 6.5 unit cell crystallite dimension, with little or no real change in crystal size. Relative lattice parameter fluctuations have been shown to decrease significantly through the LCP phase transition from a value near 2% to a value well below 1%. It may even be possible to relate this feature to an order parameter. The variations in displacement disorder also contribute to the observed peak profiles. Displacement disorder has been shown to peak near the LCP phase-transition temperature, suggesting a heterogeneous phase transition which occurs in all crystalline domains. Starting out with a relative minimum displacement disorder of 1.5% for 10 °C, having a maximum of ~4% near 55 °C, and then

approaching another local minimum of 2.5% before melting near 120 °C, these fluctuations in displacement disorder suggest that local structural inhomogeneities, in the form of side-chain melting, produce signatures of paracrystallinity.

Acknowledgment. The financial support by NSF DMR Grant No. DMR-9631575 (M.J.W.) is gratefully acknowledged.

References and Notes

- Hotta, S. In *Handbook of Organic Conductive Molecules and Polymers*; Nalwa, H., Ed.; J. Wiley & Sons, Ltd.: New York, 1997; Vol. 2, p. 309.
- Samuelsen, E. In *Handbook of Organic Conductive Molecules and Polymers*; Nalwa, H., Ed.; J. Wiley & Sons, Ltd.: New York, 1997; Vol. 3, p. 87.
- McCullough, R.; Ewbank, P. In *The Handbook of Conducting Polymers*, 2nd Ed.; Skotheim, T., Elsenbaumer, R., Reynolds, J., Eds.; Mercel-Dekker: New York; Basel: Hong Kong, 1997; p. 225.
- Winokur, M. J.; Spiegel, D.; Kim, Y. H.; Hotta, S.; Heeger, A. J. *Synth. Met.* **1989**, *28*, C419.
- McCullough, R. D.; Tristram-Nagle, S.; Williams, S. P.; Lowe, R. D.; Jayaraman, M. *J. Am. Chem. Soc.* **1993**, *115*, 4910.
- Warren, B. E.; Averbach, B. L. *J. Appl. Phys.* **1951**, *21*, 595.
- Hindeleh, A.; Hosemann, R. *J. Phys. C* **1988**, *21*, 4155.
- Hosemann, R. *Z. Phys.* **1950**, *128*, 465.
- Hosemann, R.; Schmidt, W.; Fischer, A.; Balta-Calleja, F. *An. Fis. Ser. A* **1983**, *79*, 145.
- Bonart, R.; Hosemann, R.; McCullough, R. *Polymer* **1963**, *4*, 199.
- Somashekar, R.; Somashekarappa, H. *J. Appl. Crystallogr.* **1997**, *30*, 147.
- Warren, B. E.; Averbach, B. L. *J. Appl. Phys.* **1952**, *23*, 497.
- Warren, B. E. *X-ray Studies of Deformed Metals*; Pergamon Press: New York, 1959; Vol. 8.
- Warren, B. E. *X-ray Diffraction*; Dover: New York, 1969.
- Balzar, D. *J. Appl. Cryst.* **1992**, *25*, 559.
- Balzar, D.; Ledbetter, H. *J. Appl. Cryst.* **1993**, *26*, 97.
- Balzar, D. *J. Res. Natl. Inst. Stand. Technol.* **1993**, *98*, 321.
- van Berkum, J.; Delhex, R.; Keijsers, T. D.; Mittemeijer, E. *Acta Crystallogr.* **1996**, *A52*, 730.
- Schneider, M.; Zeiger, W.; Worch, H.; Schumann, J.; Biscourp, P.; Lange, G. *Mater. Sci. Forum* **1996**, *225–227*, 191.
- Ungár, T.; Borbély, A. *Appl. Phys. Lett.* **1996**, *69*, 3173.
- Bimbauld, L.; Badawi, K.; Goudeau, P.; Branger, V.; Durand, N. *Thin Solid Films* **1996**, *275*, 40.
- Mestl, G.; Herzog, B.; Schögl, R.; Knözinger, H. *Langmuir* **1995**, *11*, 3027.
- Enzo, S.; Polizzi, S.; Benedetti, A. *Z. Kristallogr.* **1985**, *170*, 275.
- Lin, J.-D.; Duh, J.-G. *J. Mater. Sci.* **1997**, *32*, 5779.
- Lin, J.-D.; Duh, J.-G. *J. Mater. Sci.* **1997**, *32*, 4901.
- Lanson, B.; Kubler, B. *Clays Clay Miner.* **1994**, *42*, 489.
- Bodor, G. *Adv. Polym. Sci.* **1985**, *67*, 165.
- Howard, P. R.; Crist, B. *J. Polym. Sci., Polym. Phys. Ed.* **1989**, *27*, 2269.
- Crist, B.; Howard, P. R. *Adv. X-ray Anal.* **1991**, *34*, 519.
- Tashiro, K.; Kobayashi, K.; Kawai, T.; Yoshino, K. *Polymer* **1997**, *38*, 2867.
- Leclerc, M.; Faid, K. In *The Handbook of Conducting Polymers*, 2nd ed.; Skotheim, T., Elsenbaumer, R., Reynolds, J., Eds.; Mercel-Dekker: New York; Basel: Hong Kong, 1997; p. 695.
- Chen, S.-A.; Ni, J.-M. *Macromolecules* **1992**, *25*, 6081.
- Zhao, Y.; Yuan, G.; Roche, P.; Leclerc, M. *Polymer* **1995**, *36*, 2211.
- Park, K.; Levon, K. *Macromolecules* **1997**, *30*, 3175.
- Tashiro, K.; Ono, K.; Minagawa, Y.; Kobayashi, M.; Kawai, T.; Yoshino, K. *J. Polym. Sci., Polym. Phys.* **1991**, *29*, 1223.
- Prosa, T. J.; Winokur, M. J.; Moulton, J.; Smith, P.; Heeger, A. J. *Macromolecules* **1992**, *25*, 4364.
- Bunn, C. *Trans. Faraday Soc.* **1939**, 482.
- Busing, W. R. *Macromolecules* **1990**, *23*, 4068.
- Jordan, E.; Feldeisen, D.; Wrigley, A. *J. Polym. Sci.* **1971**, *9*, 1835.
- Yang, C.; Orfino, F.; Holdcroft, S. *Macromolecules* **1996**, *29*, 6150.

- (41) Alexander, L. E. *X-ray Diffraction Methods in Polymer Science*; Wiley Interscience: New York, 1969.
- (42) Plate, N. A.; Talrose, R. V.; Freidzon, Y. S. *Polym. J.* **1987**, *19*, 135.
- (43) Inganäs, O.; Salaneck, W. R.; Osterholm, H.; Laakso, J. *Synth. Met.* **1988**, *22*, 395.
- (44) Moulton, J.; Smith, P. *Synth. Met.* **1991**, *40*, 13.
- (45) Moulton, J.; Smith, P. *Polymer* **1992**, *33*, 2341.
- (46) Leclerc, M.; Diaz, F. M.; Wegner, G. *Makromol. Chem.* **1989**, *190*, 3105.
- (47) Certain commercial materials and equipment are identified in this paper in order to adequately specify the experimental procedure. In no case does such identification imply recommendation by the National Institute of Standards and Technology nor does it imply that the material or equipment identified is necessarily the best available for this purpose.
- (48) Ergun, S. *J. Appl. Crystallogr.* **1968**, *1*, 19.
- (49) Caglioti, G.; Paoletti, A.; Ricci, F. P. *Nucl. Instrum.* **1958**, *3*, 223.
- (50) The values used for deconvolution of instrument from spectra are as follows: $U_{\alpha_1} = -0.261$, $V_{\alpha_1} = 0.0577$, $W_{\alpha_1} = 0.0388$, $U_{\alpha_2} = 0.0238$, $V_{\alpha_2} = 0.0119$, and $W_{\alpha_2} = 0.0218$.
- (51) Takahashi, H. *J. Phys. Soc. Jpn.* **1969**, *27*, 708.
- (52) Crist, B.; Cohen, J. B. *J. Polym. Sci., Polym. Phys. Ed.* **1979**, *17*, 1001.
- (53) Guinier, A. *X-ray Diffraction in Crystals, Imperfect Crystals, and Amorphous Bodies*; W.H. Freeman: San Francisco, 1963.
- (54) Vogel, W.; Haase, J.; Hosemann, R. *Z. Naturforsch.* **1974**, *29a*, 1152.
- (55) Cowley, J. M. *Acta. Crystallogr. A* **1976**, *32*, 83.
- (56) Bertaut, E. *Acta. Crystallogr.* **1952**, *5*, 117.
- (57) Young, R.; Gerdes, R. J.; Wilson, A. *Acta. Cryst.* **1967**, *22*, 155.
- (58) Rothman, R. L.; Cohen, J. B. *Adv. X-ray Anal.* **1969**, *12*, 208.
- (59) Delhez, R.; DeKeijser, T. H.; Mittemeijer, E. *Fresenius Z. Anal. Chem.* **1982**, *312*, 1.
- (60) Delhez, R.; deKeijser, T.; Mittemeijer, E. J. *Natl. Bur. Stand. Spec. Pub.* **1980**, *567*, 213.
- (61) Prosa, T. J.; Winokur, M. J.; McCullough, R. D. *Macromolecules* **1996**, *29*, 3654.
- (62) Bolognesi, A.; Catellani, M.; Destri, S.; Porzio, W. *Makromol. Chem., Rapid Commun.* **1991**, *12*, 9.
- (63) Bolognesi, A.; Porzio, W.; Provasoli, F.; Ezquerra, T. *Makromol. Chem.* **1993**, *194*, 817.
- (64) Bolognesi, A.; Porzio, W.; Zjuo, G.; Ezquerra, T. *Eur. Polym. J.* **1996**, *32*, 1097.
- (65) Meille, S. V.; Romita, V.; Caronna, T.; Lovinger, A. J.; Catellani, M.; Belobrzechkaja, L. *Macromolecules* **1997**, *30*, 7898.
- (66) Press, W. H.; Teukolsky, S. A.; Vetterling, W. T.; Flannery, B. P. *Numerical Recipes in Fortran: The Art of Scientific Computing*; Cambridge University Press: New York, 1992.
- (67) Wecker, S.; Cohen, J.; Davidson, T. *J. Appl. Phys.* **1974**, *45*, 4453.
- (68) Buchanan, D. R.; Miller, R. L. *J. Appl. Phys.* **1966**, *37*, 4003.

MA981059H